A STUDY OF SOME TRANSVERSAL MOTIONS OF THE ELECTRON BEAM OF A LINAC

R. BERGERE and A. VEYSSIERE
Département de Recherche Physique
Centre d'Etudes Nucléaires de SACLAY
B.P. N° 2 - GIF-sur-YVETTE - (S et O) FRANCE -

ABSTRACT : It is well known that when the magnetic focusing field at the input of an electron linac increases the output accelerated current does not increase regularly. Such a behaviour is shown to be connected with rotations, in the output plane of the linac, of the center of charges of the beam. These rotations have been displayed experimentally by means of a beam position monitoring system and related to the transverse momentum transferred to the beam by the spurious TM_{11} mode existing in the mode converter which changes at the input of the Saclay linac, the TE_{01} mode from the rectangular waveguide into a TM_{01} mode on the accelerator circular waveguide.

INTRODUCTION

It is a well known phenomenon that, for an electron linac, the proper choice of the axial magnetic focussing field, does not follow a simple law. More precisely, experimental results (1,2) have shown that the actual accelerated electron beam intensity does not increase regularly with an increasing focalising magnetic field. Several minima and maxima of accelerated electron beam current can easily be detected for an increasing focalising field. As far as the linac of 1 GEV at ORSAY is concerned, a theoretical explication of this phenomenon has been proposed (3) it considers, in the case of a slightly off center injected electron beam, some resonance phenomena by coupling of axial and radial oscillations.

I. EXPERIMENTAL OBSERVATIONS

Let us start with a schematic representation of the linac at Saclay. The total focalising magnetic field is created by 3 sets of coils so that $B_z(\text{total}) = B_1(z) + B_2(z) + B_g(z)$. At the end of each section we have arranged the following detecting devices :1°) Two electron beam current monitors, (I_1 and I_2) (ferrite transformer or a UHF cavity detector) (4). 2°) Two beam position monitors (P_1 and P_2) consisting of four appropriately coupled microwave loops, described in detail in another paper (5). 3°) At the end of the last section we have an additional isolated electron beam collimator having a diameter of 19 mm. This allows us to obtain some information as to that part of our electron beam which leaves the accelerator at a distance 9,5 mm. from its axis.

The experimental data thus obtained can be put succinctly as follows ; keeping parameters B_1, B_2 and all other machine parameters and especially the injected electron beam constant, we observe that the beam current behaves as indicated below when varying (B_g) ; a) At the end of the first section ($E_{electrons}$ = 14 MeV) the beam current I_1 increases rapidly with increasing (B_g) till it attains a steady maximum value (Fig. 1a).b) At the end of the second section ($E_{electrons}$=28MeV) the beam current I_2 shows a series of marked maxima and minima (Fig. 1b). c) Also at the end of the second section, the current collected by our additional collimator (I_{ex}) shows the analogous minima and maxima as those observed for I_2 but their positions are exchanged (Fig. 1c). This suggests the idea that the maximum current emerging from the accelerator must correspond to a well centered beam. This was confirmed by visual observation of the center of gravity of a section of our electron beam on a scope connected to the beam monitoring device P_2 (or P_1). We do in fact observe as many rotations of this center of gravity as there are periods on the graphs $I_2 = f(B_g(z))$ where each maximum M_1, M_2, M_3, M_4 corresponds to a well centered and each minimum m_i to a badly centered emerging electron beam. (Fig. 2).

Hence we concluded that the phenomenon to be studied was basically the rotation of the center of gravity of a section of the emerging accelerated electron beam, in a plane perpendicular to the axis of the accelerator.

II. ORIGIN OF ROTATIONS

Clearly these rotations are associated with transverse movements of the electrons constituting the beam. Such movements, when they exist, cannot be solely caused by the E_{radial} component of the TM_{01} mode in the accelerator itself, since $E_r = 0$ on the axis. In order to

explain such transverse electron movements, we therefore need either of the following : a) an initial distance between the accelerator axis and the electron itself, thus annuling condition $E_r = 0$. b) an initial transverse velocity, caused by a yet to be determined force, which produces an eventual divergence from the axis. Several sources of such initial transverse velocities exist and we shall briefly investigate each of them.

A/Terrestrial magnetic field.

Let us consider electrons injected with an axial velocity of 0.3 c which corresponds roughly to our standard operating conditions. These electrons of (20-30) KeV have to traverse about 10 cm before reaching B_1. This gives us an approximate transverse velocity of

$$v_{trans}(r) = \frac{eB}{m}\ell = 3.10^{-3}c$$

But this is at least ten times smaller than the value required to interpret our results as we shall see later.

B/ The gradient of the axial magnetic field.

Since the cathode of the electron gun is shielded from any exterior magnetic field, the emerging electrons enter suddenly into the region of B_1 where a field of about 500-600 Gauss exists. Applying Busch's theorem, and supposing the coordinate systems of our magnetic fields and our accelerated particles to coincide, we find the following initial angular velocity for our electrons when entering the accelerator :

$$\left(\frac{d\theta}{dt}\right)_z = \frac{e}{mr_0^2}\left(r_2 A_{\theta 2} - r_1 A_{\theta 1}\right) = \frac{e}{m}\frac{1}{2\pi r_0^2}\left(\varphi_2 - \varphi_1\right)$$

The transverse velocity distribution at the beginning of the accelerator shall thus be represented by a vector velocity diagram having the same axial symmetry as the magnetic field causing it. This symmetric effect, however, associated with the symmetry of the TM_{01} mode existing in the accelerator, does not explain the nonsymmetric rotations executed by the center of gravity of the electron beam at the end of the section II. Furthermore, disregarding these symmetry considerations for a moment, subsequent calculations show clearly that all electrons entering the accelerator with transverse velocities greater than $(\frac{c}{20})$ do not emerge from the first section at all. But comparing this value with the transverse velocity acquired by an electron at r = 3 mm, say, due to the magnetic field gradient we find :

$$r\left(\frac{d\theta}{dt}\right) = v_{trans.\ r=3mm} = r\left(\frac{eB}{2m}\right) = c/23 \quad \text{for B = 500 gauss}$$

Thus we see that only electrons having r < 3 mm. at the entrance of the accelerator could possibly be considered, and even this possibility is to be rejected due to the above mentioned symmetry considerations.

C/ TM_{11} mode in input coupler.

It is well known that the input coupler, situated at the entrance of a linear accelerator and which is supposed to convert the incoming TE_{01} mode from a rectangular waveguide into a TM_{01} mode for a circular waveguide, also introduces a certain amount of dissymmetry into the configuration of the emerging field (6,7). These parasitic effects have been calculated for long accelerators by R.H. Helm (8). The essence of the method is the assumption that a second superimposed field, namely a TM_{11} mode exists having a plane of symmetry coinciding with the axis of the rectangular waveguide.

This assumption corresponds with our observations of discharge effects caused by multipactor electrons. This multipactoring effect is occurring in a standing wave pattern originating in a mismatch of the end cavities of the first section. On the walls of these cavities a succession of alternating ring discharges caused by such multipactor electrons can clearly be seen. The odd cavities have wide discharge rings (E_z direct + E_z inverse) and the even cavities narrow rings (E_z direct - E_z inverse). This corresponds exactly to an axially symmetric standing wave pattern based on a TM_{01} mode for a phase difference of $\frac{\pi}{2}$ between cavities (Fig. 3a). However on the inside of the input coupler (Fig. 3b) we find a discharge ring without any axial symmetry but with a plane of symmetry passing through the axis of our rectangular waveguide. Such a figure corresponds exactly to the superposition of the electric fields $E_z(r)$ of the normal TM_{01} mode and the parasitic TM_{11} mode. We note here that this TM_{11} mode can only exist at the height of the input coupler itself since the cut-off for the accelerator is greater than the accelerating frequency of 3000 MHz. A more detailed analysis of the fields involved shows clearly that beyond the second cavity we have a pure TM_{01} mode and a superposition of TM_{01} and TM_{11} modes between the entrance of the input coupler and the second cavity.

Putting $\theta = 0$ as being the axis of symmetry of the TM_{11} mode, we can write approximately for the total longitudinal electric field :

$$E_{z\,total}(r,\theta) = E_{z01} J_0\left(\frac{2\pi r}{\lambda_{c01}}\right) + E_{z11}\cos\theta\, J_1\left(\frac{2\pi r}{\lambda_{c11}}\right)$$

But even electrons entering the accelerator exactly along the axis will be subject, not only to the above mentioned longitudinal accelerating field, but simultaneously to the E_x and E_y components of the same parasitic TM_{11} mode. We shall now try and give some definite values to these new parameters. For the cavity adjacent to the volume (AA') of the input coupler we measured the following ratio:

$$1,15 = \frac{[H_{\theta(01)} + H_{\theta(11)}]_{\theta=0°}}{[H_{\theta(01)} + H_{\theta(11)}]_{\theta=180°}} \quad \text{hence} \quad \frac{H_{011}}{H_{001}} = 0,07$$

Taking the attenuation due to the distance between (AA') and the first cavity into account and using standard classical equations in cylindrical coordinates for modes TM_{01} and TM_{11} we obtain finally the ratio $\frac{E_{11}}{E_{01}}$ for the interaction volume AA' of the input coupler. The following results also ensue :

$$\left(\frac{E_{11}}{E_{01}}\right)_{AA'} = 2\left(\frac{H_{011}}{H_{001}}\right)\exp\left[2\pi\frac{\Delta x}{\lambda g}\right] = 1/5.3$$

$$E_r(r=0,\theta=0) = E_x = -j\frac{\lambda c_{11}}{\lambda g}\frac{E_{01}}{5.3}J_1'\left(\frac{2\pi r}{\lambda c_{11}}\right)$$

$$H_r(r=0,\theta=\tfrac{\pi}{2}) = H_y = -j\sqrt{\frac{\varepsilon}{\mu}}\frac{\lambda c_{11}}{\lambda}\frac{E_{01}}{5.3}J_1\left(\frac{2\pi r}{\lambda c_{11}}\right)\Big/\frac{2\pi r}{\lambda c_{11}}$$

Since the TM_{11} mode is strongly attenuated, the corresponding wavelength inside the waveguide is imaginary. Thus E_x and H_y are 90 degrees out of phase, and E_x will be in phase with the longitudinal field $E_{z(11)}$ and consequently with the field $E_{z(01)}$ on the axis. This is confirmed by the configuration of the multipactor discharge ring (Fig. 3). Further, from reference (9) we know that E_{01} = 80 Kilovolts cm^{-1}, and hence we can find E_x and H_y for r = 0 :

E_x = 5,2 KV cm^{-1} hence $F_E = F_{Ex} = 8,3.10^{-14}$ Newton

H_y = 1,4 At m^{-1} $F_M = F_{Mx} = 2,8.10^{-14}$ Newton

Thus the transverse velocities acquired by electrons in passing through the critical interaction volume AA' shall be approximately those due to the electric field alone :

$V_{trans} = \left(\frac{Fe}{m}\right)\Delta t \simeq \frac{c}{46}$ in good agreement with the value $\frac{c}{38}$ required in the next computations.

III. THEORETICAL ANALYSIS.

A theoretical analysis of electron movements for electrons having a certain amount of transverse velocity at the moment of their injection into the accelerator, has been performed by means of an analogue computer. (10) The following set of equations has been solved :

$$\frac{d^2z}{dt^2} = \frac{e}{m}E_0\cos\varphi \qquad m = \frac{m_0}{\left[1 - \frac{1}{c^2}\left(\frac{dz}{dt}\right)^2\right]^{3/2}}$$

$$\frac{d\varphi}{dt} = \left(\frac{dz}{dt} - V_\varphi\right)\frac{\omega}{V_\varphi}$$

$$\frac{d}{dt}(m'x') = \frac{-e\omega}{V_\varphi}\frac{E_0}{2}\sin\varphi\left[1 - \frac{V_\varphi}{c^2}\frac{dz}{dt}\right]x - eBy'$$

$$\frac{d}{dt}(m'y') = \frac{e\omega}{V_\varphi}\frac{E_0}{2}\sin\varphi\left[1 - \frac{V_\varphi}{c^2}\frac{dz}{dt}\right]y + eBx'$$

where $m' = m_0\left[1 - \left(\frac{1}{c}\frac{dz}{dt}\right)^2\right]^{-1/2}$

V_φ = phase velocity

The parameters $E_0(z)$ $V_y(z)$, and $B(z) = f.B_1 + g.B_2 + h.B_g(z)$ are fixed by the actual construction details of the accelerator. An increase of Bg(z) at all points along the axis could be represented by varying h between 1 and 4. This variation of (h) corresponds to a change from 300 to 1200 Gauss in the value of B(z) at the point where the field is a maximum.

A/ Behaviour of a typical "average electron"

A previous analysis concerned mainly with longitudinal effects (11, 12, 13) caused by the disturbing influences of the AA' space of the input coupler, before the input of the buncher itself has shown that we can define for each bunch an average electron with parameters :

$$\langle\varphi_0\rangle \simeq 0 \; ; \; \langle\beta_0 c\rangle \simeq 0,5c \; ; \left(\frac{dz}{dt}\right)_0 = \frac{c}{40} \; ; \left(\frac{dy}{dt}\right)_0 = 0$$

$$x_0 = y_0 = 0$$

We now determine the transverse movements of such an average electron for different field conditions in the buncher and accelerator by varying (h) from 1 to 4. This corresponds to the actual experiment where we vary the current in the coils producing field (Bg) and observe the path traced by the center of gravity of a section of the electron beam at the end of section I or II. We thus obtain a number of points corresponding to different values of (h), each of which represents the center of gravity of the beam for which the average electron has been defined above. Fig. 4a represents these theoretical rotations calculated till the end of section I. These theoretical curves show a good agreement with the corresponding experimental values shown in (Fig. 4 b).

B/ Evolution of an "Average electron beam cross section".

Let us now try to gain some insight in the evolution of an elementary "average electron beam cross section" for any given magnetic field configuration (f, g, h all constant). Let us define such an average cross section by means of 4 electrons situated at the periphery

of the electron beam section, the section itself being defined by our above mentioned average electron. We can thus obtain, for any value of z, the transverse changes of such an average section of the electron beam by drawing a circle passing as close as possible through the 4 points representing the transverse movements of these four typical electrons. Fig.5 a shows the results of such a computation for h = 2 and from the entrance of the buncher till z = 6 m. Similar results are shown for h = 3 and h = 4 in Fig. 5 b and Fig. 5 c(Very similar to the results obtained for beams of non relativistic electrons (14,15)).

C/ Study of individual electrons constituting an elementary bunch.

A previous study of the movements of individual electrons contained in an elementary bunch (12) has allowed us to determine a set of coupled parameters (γ_{oi} ; $\beta_{oi}c$) valid at the entrance of the buncher for about 20 electrons representing an elementary bunch. If we compute for each electron the transverse momentum $(\frac{dx}{dt})$ gained when passing through the input coupler and consider that all our representative electrons enter on the axis, ($y_{oi} = x_{oi} = 0$ for all i), we then obtain for a given magnetic field configuration (h = 2, g = constant, f = constant) the theoretical transverse movement of each of these electrons and hence of the whole bunch itself. The transverse distribution of these electrons is shown in Fig. 6 a for the end of the first section and in Fig. 6 b for the end of the second section. We can now repeat the calculations for another set of twenty electrons entering, say, at a distance of 2 mm from the axis. The additional results obtained from Fig. 5 allow us to regard each of the final positions of our twenty representative electrons as the center of an average section of the beam. Hence by drawing the appropriate circles D_1 = 11 mm.and D_2= 14,6 mm. representing the respective average diameters of the electron beam at the end of sections I and II, we finally obtain Fig. 6 c and Fig. 6 d, showing the actual average transverse extension of the electron beam at the sites in question.(Numbers on Fig. 6 indicate sequence of arrival within a bunch of the 19 representative electrons).

D/ Accelerated currents at the end of Sections I and II.

We now are in a position to interpret the electron beam current at the end of sections I and II respectively. We have seen that I_1 and I_2 are both fonctions of $B_{z(total)}$. Since h controls B_g and we have B_1 and B_2 constant, we can write $I_1 = F(h)$ and $I_2 = S(h)$. We here associate with each average electron (whose position is fixed in the transverse plane as shown in Fig. 4 a) the appropriate circle representing the cross section of the average electron beam at the appropriate value of z as is shown in Fig. 6 c and Fig. 6 d. We thus obtain Fig. 7 a and Fig.7 b where A represents the area corresponding to the surface of the appropriate beam diameter D (h) and A', the hatchured surface, represents the electrons which are intercepted by the iris itself. It follows from Fig. 7 a and Fig. 7 b that the actual emerging electron beam current I_1 is given by $I_1 = I_o \frac{A - A'}{A}$. This reduces to $I_1 = I_o \frac{A}{A'} = I_o$ for all $h \gg 1,7$. The final result of this part of our analysis can best be summarized by means of Fig. 8 which shows, the theoretical current at the end of section I, I_1 in full lines compared with the experimental results shown in dotted lines. Fig. 9 shows an identical analysis applied to current I_2 at the end of section II. We see that our theoretical results confirm and explain our experimental curves fairly well, and more specifically they interpret with good accuracy the interval $\Delta(h) = \Delta B_z$ separating two successive current maxima or minima. Further it becomes clear that the collimator at the end of section II, which has a smaller diameter than the one of the last accelerator iris, shall intercept a current (I_{ex}) proportional to $I_o \frac{A'}{A}$. This explains the graph of Fig. 1 c.

E/ Fine structure of I (h).

Fig. 10 a shows three typical accelerating fields, $E_{o\,(a)}(z)$, $E_{o\,(b)}(z)$ and $E_{o\,(c)}(z)$, (with beam loading), all along the first section. These fields replace our standard field E_o (z) when we vary the power output of Klystron I delivering power to the buncher. Substituting any one of these new accelerating electric field parameters into our equations of motion, we obtain a new set of nearly identical rotations indicated in Fig. 10 b, the whole new set being slightly displaced with respect to the original one. Hence the law I_2 (h) of Fig. 10 c which agrees well with the experimental values shown in Fig. 10 d. In fact experimental data indicates a sliding movement of the maxima as a function of the accelerating fields giving: $\frac{dh\ max}{h\ max} \frac{d\ Eoz}{Eoz} = 0,50 \pm 0,10$ where theoretical calculations represented by Fig. 10 c give the value of 0,53 for the same quantity.

F/ Fine structure of rotations.

When the power supply of the coils creating the focalising magnetic field is not very stable, there appears a 50 Hz ripple on the $B_g(z)$ field. As far as the electron pulses are concerned, an accelerator functionning at 500 pulses per second, synchronised with the net, shall therefore exhibit 10 different values of $B_g(z)$. Thus for this given pulse rate, the beam should have 10 different transverse positions for any given fixed focusing field (f, g and h constant). This phenomenon does indeed occur on the scope associated with the position monitor.

REFERENCES

1°)T.N. FILIMONOVA and A.M.SHMYGOV
A 15 MeV electron linear accelerator
Soviet Physics-Technical Physics Vol.7
N° 12, June 1963, p.1002.

2°)Rapport d'activité de l'accélérateur linéaire d'ORSAY du 15 Novembre 1960.
Faculté des Sciences d'Orsay - France.

3°)H. LEBOUTET
Problèmes physiques de la construction de l'accélérateur 1 GEV d'Orsay.
L'Onde Electrique, Juin 1963, p.599 à 622.

4°)R. BERGERE, E. DELEZENNE et A.VEYSSIERE
Etude de moniteurs de courant pour un accélérateur linéaire d'électrons.
Nuclear Instruments and Methods 15 (1962) p.327-354.

5°)R. BERGERE, A. VEYSSIERE and P. DAUJAT
Linac beam position monitor
The Review of Scientific Instruments
Vol. 33 n° 12 1441-1449 Décembre 1962.

6°)International Conference on High Energy Accelerators
TID 7636, p. 83.

7°)Two miles accelerator project
SLAC report n° 32 Octobre 1964.

8°)R.H. HELM
Effects of stray magnetic fields and R.F. coupler asymmetry.
SLAC n° 20, Octobre 1963.

9°)R. BERGERE et A. VEYSSIERE
Accélération dans un accélérateur d'électrons émis par effet de champ.
Nuclear Instruments and Methods 30 (1964) 309-330.

10°)J.M. BOUQUIN et Ch. DI FALCO
Etude analogique de l'effet d'une quantité de mouvement transversale initiale sur le mouvement d'un électron accéléré.
Rapport C.Ca CA 64.20.

11°)R. BERGERE, A. VEYSSIERE, S. ROLAND
"Ondes millimétriques rayonnées par le faisceau d'électrons d'un accélérateur linéaire."
Communication faite au Vème Congrès International des tubes hyperfréquences
Paris Septembre 1964.

12°)R. BERGERE, A. VEYSSIERE et H. BEIL
"Etude du groupement des électrons dans l'accélérateur linéaire de Saclay".
Rapport C.E.A. n° 2749, CEN SACLAY, B.P. n°2 Gif-sur-Yvette. (S et O) - France.

13°)A.I.ZYKOV, E.K. OSTROVSKII and L.A. MAHNENKO, Soviet Physics, Technical Physics. Vol.8, n°9, p. 795.

14°)J.L.PALMER and C. SUSSKIND
Effects of transverse velocities in magnetically focused cylindrical electron beam
MicrowavesTubes, Münich 11 Juin 1960.

15°)G.R. BREWER
Some characteristics of a magnetically focused electron beam.
Journal of Applied Physics, Vol. 30, n° 7, July59.

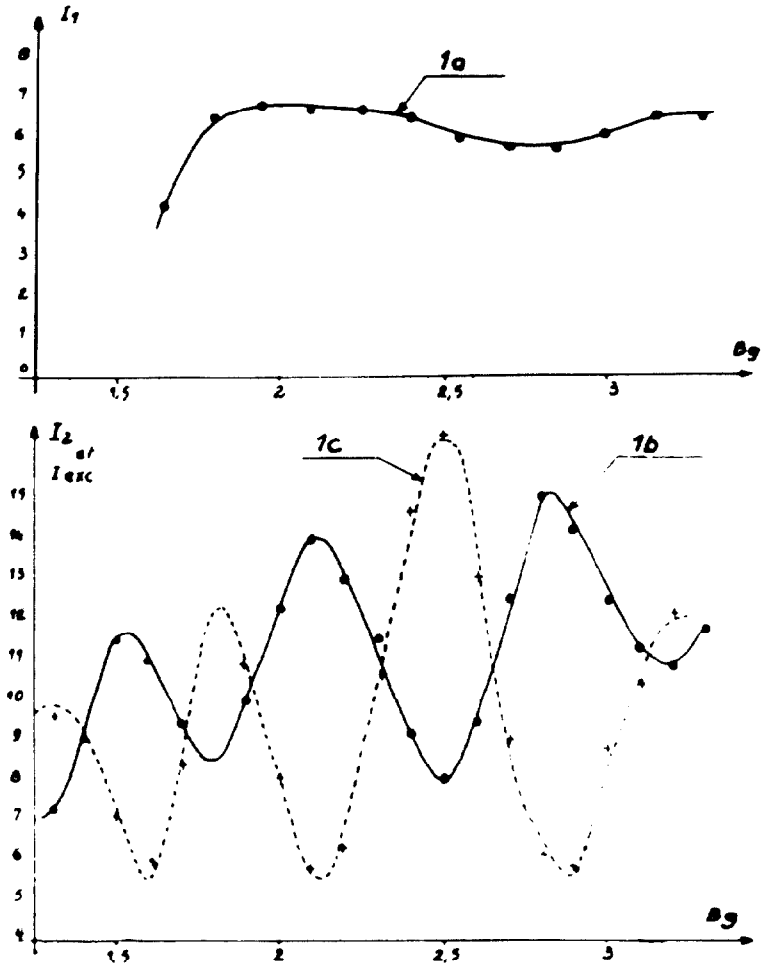

Figure 1.

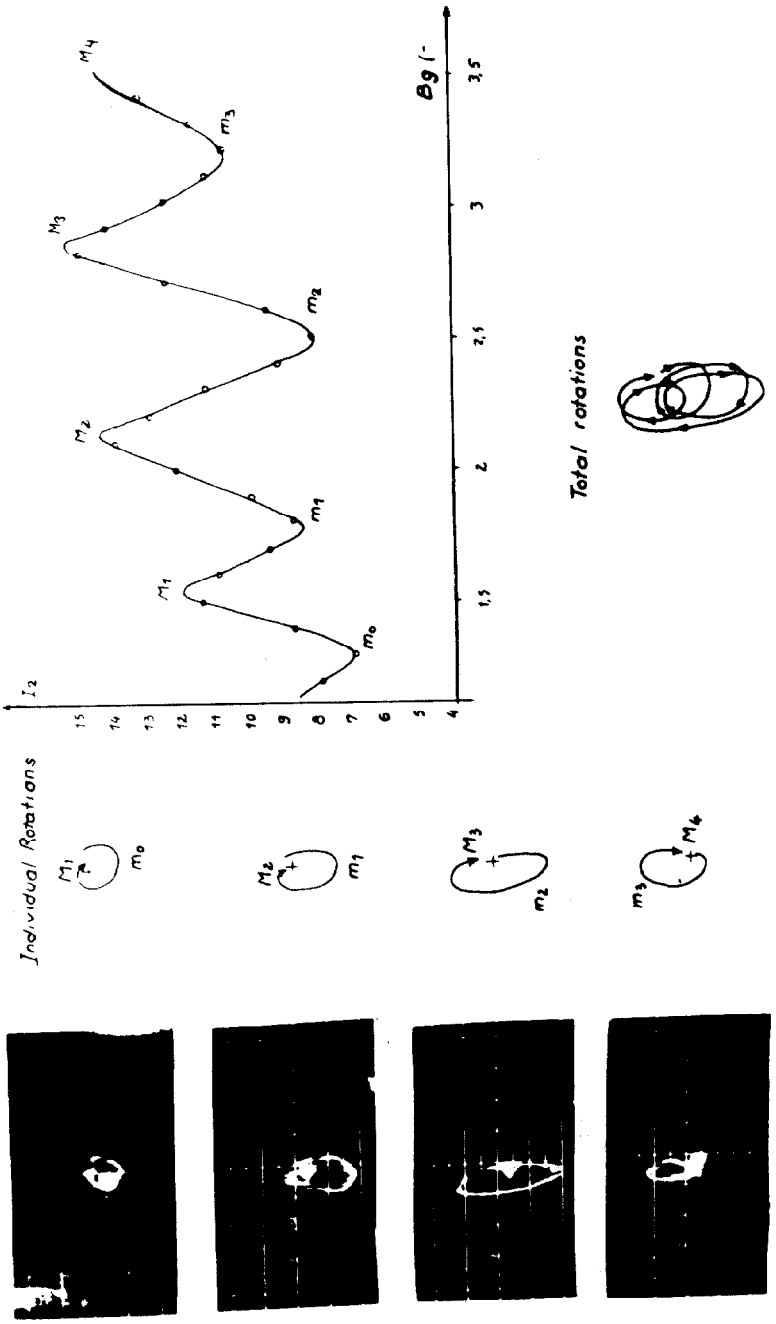

Figure 2.

Figure 3a.

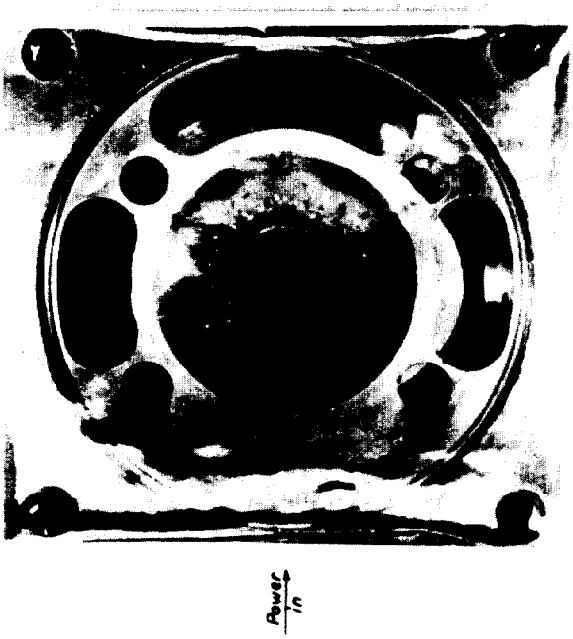

Figure 3b.

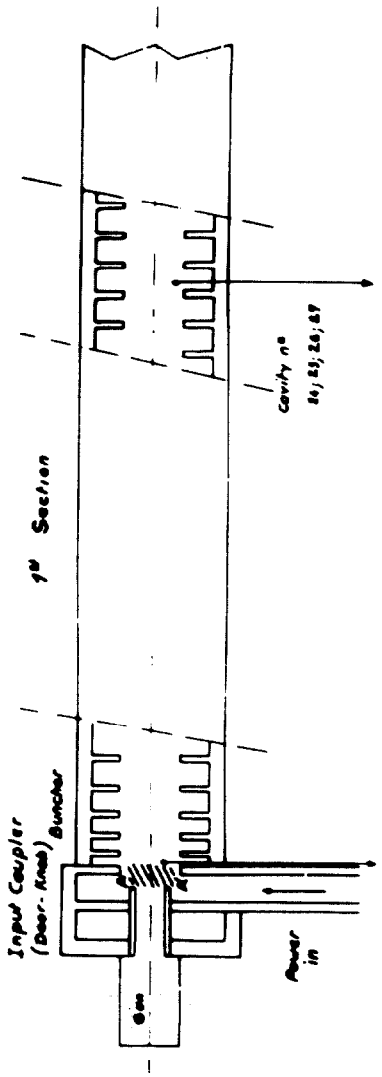

Figure 3c.

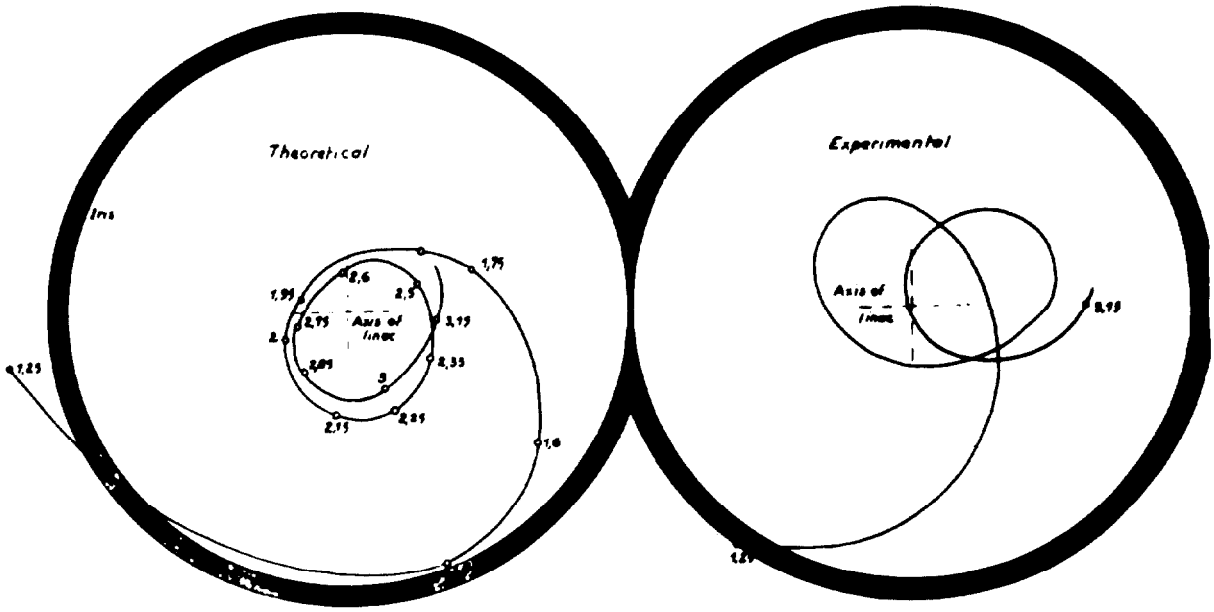

Figure 4a.

Figure 4b.

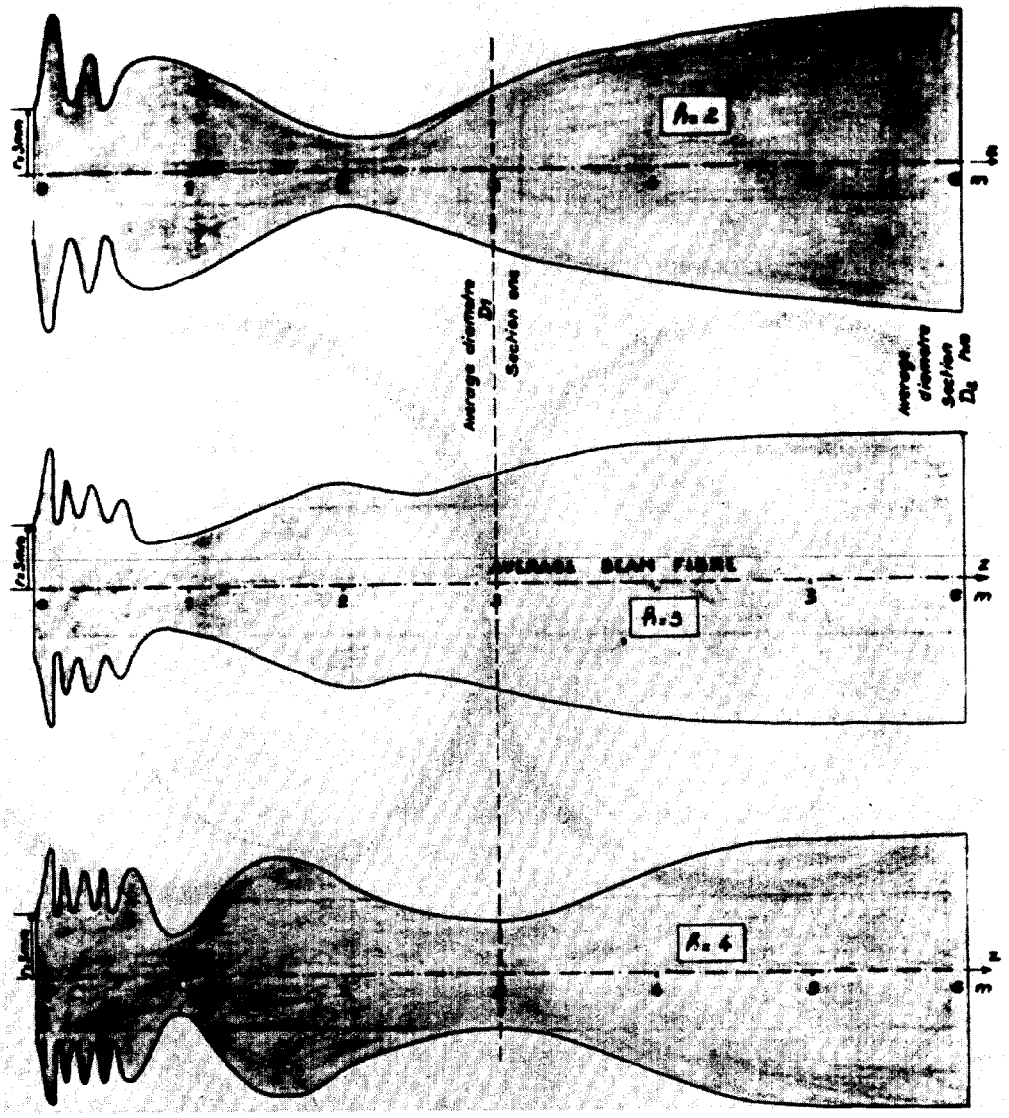

Figure 5.

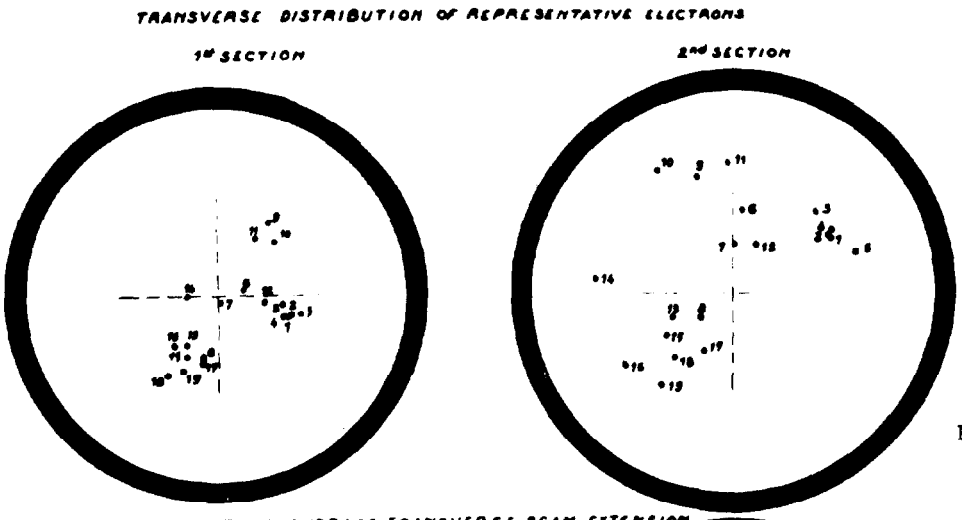

Figure 6a.

Figure 6b.

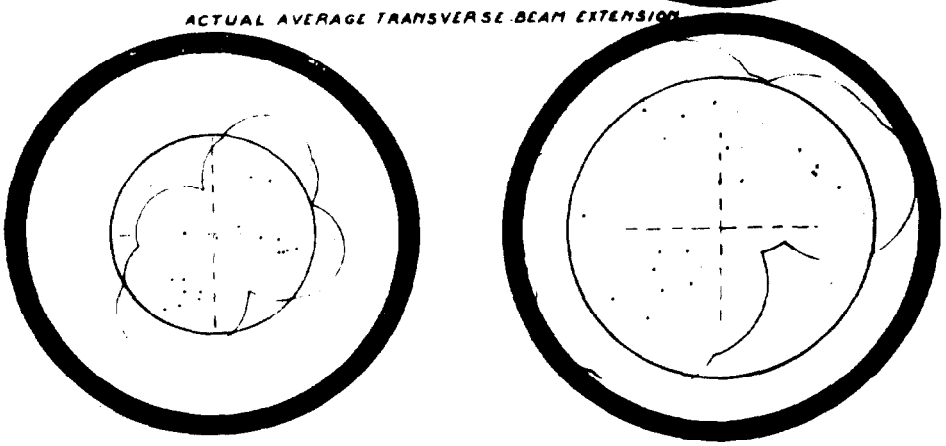

Figure 6c.

Figure 6d.

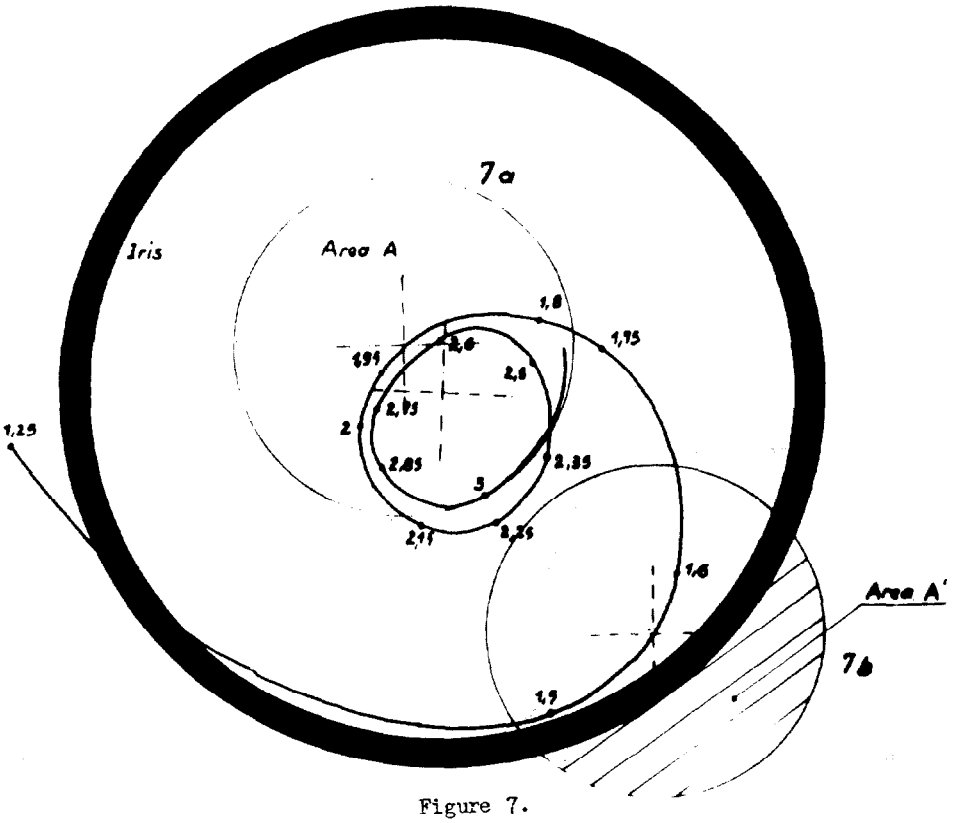

Figure 7.

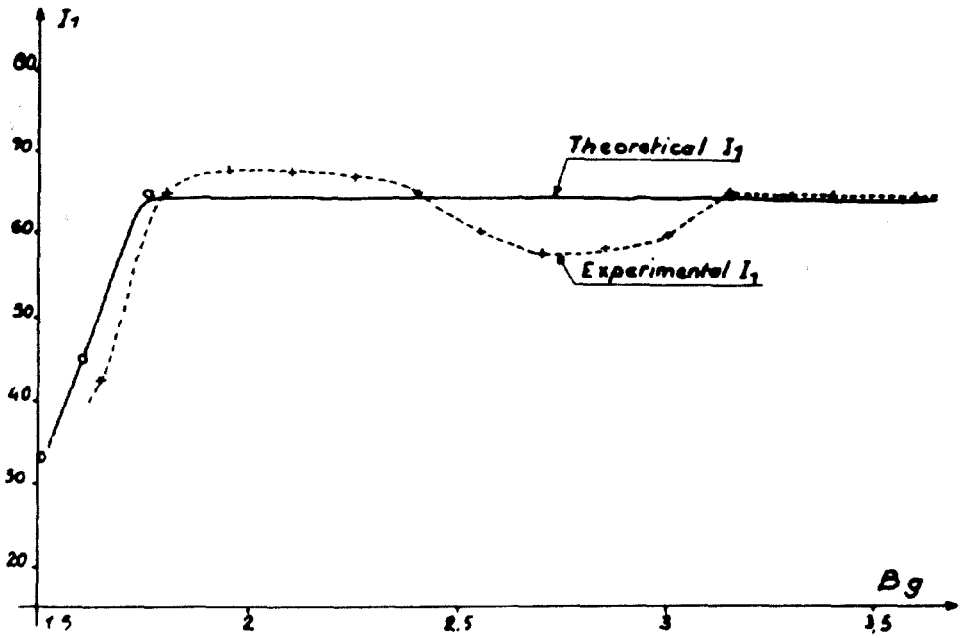

Figure 8.

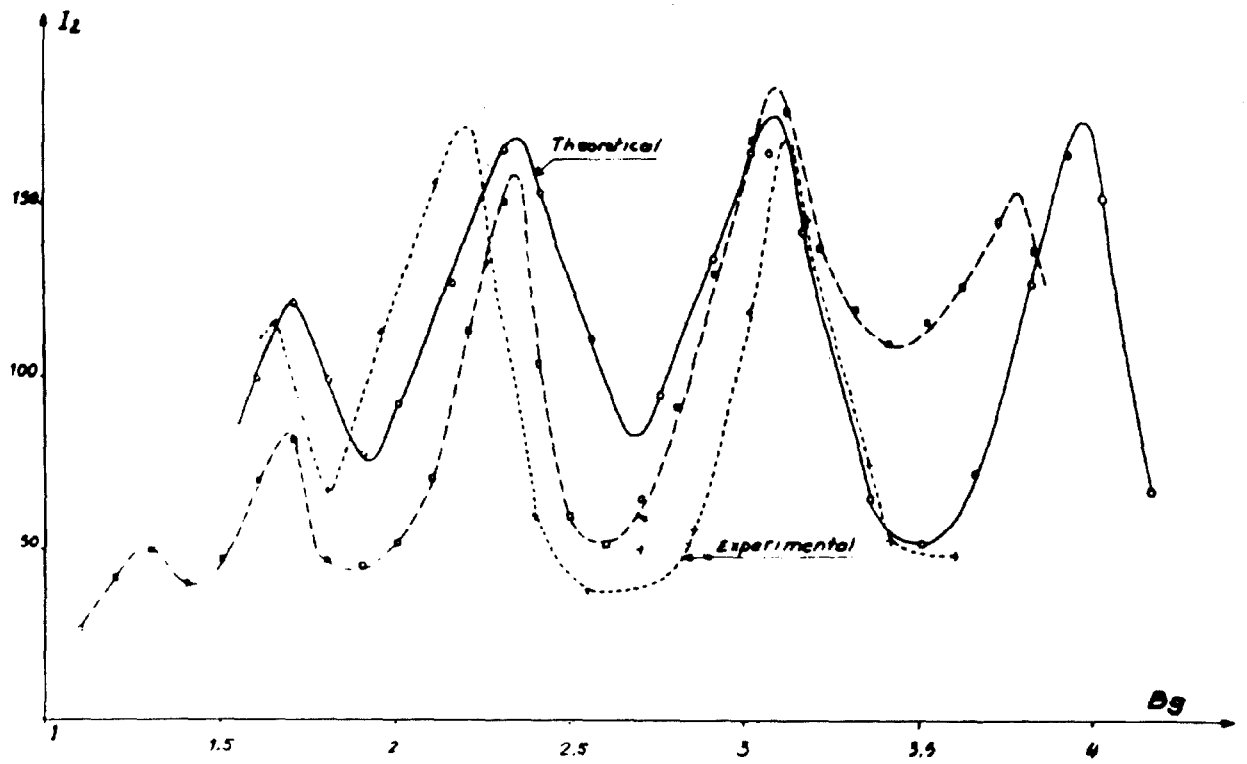

Figure 9.

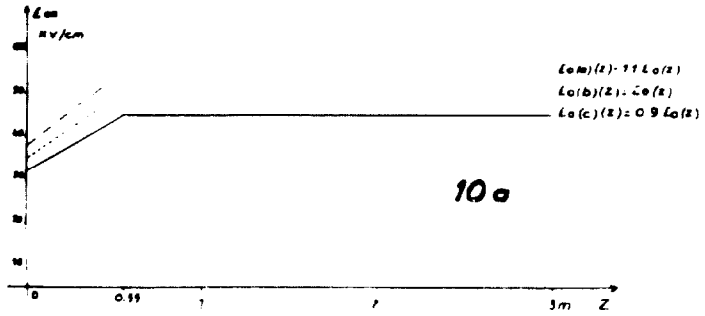
10 a
3m
Z

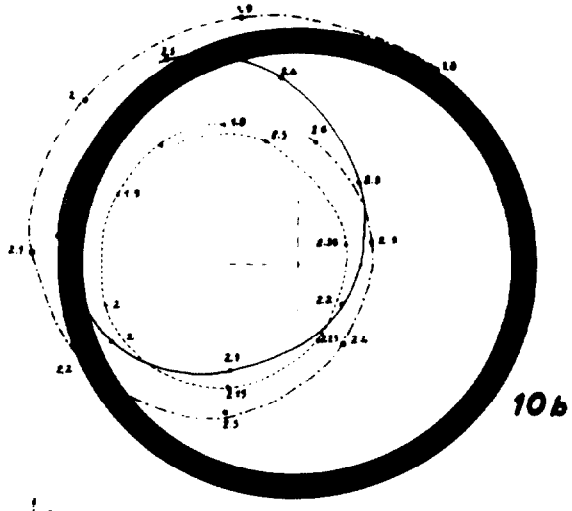
10 b

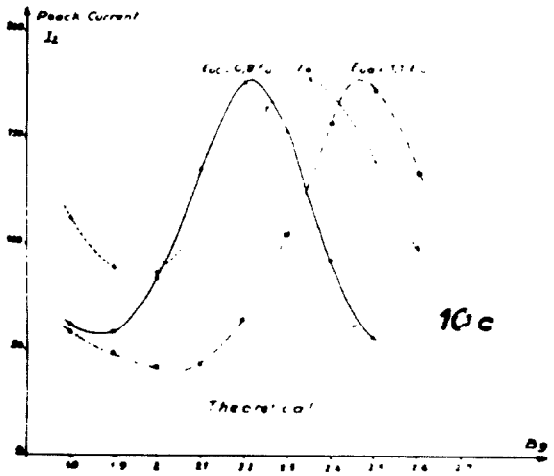
Peack Current
10 c
Theoretical

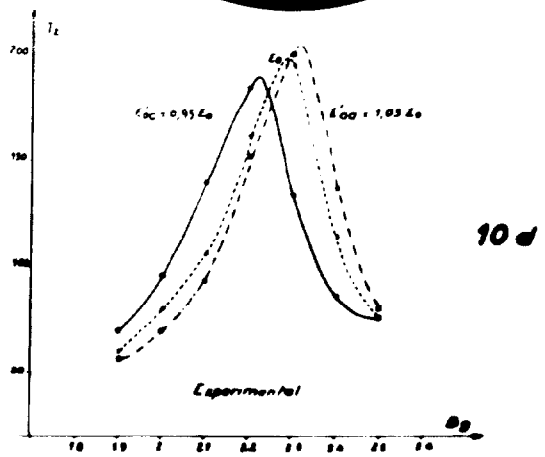
10 d
Experimental

Figure 10.